# H.E.S.S. technical note
# Gain settings for the upgraded H.E.S.S. CT1-4 cameras under moonlight observations

L. Tomankova[1], A. Yusafzai[1], D. Kostunin*[2], G. Giavitto[2], S. Ohm[2], A. Mitchell[1], M. de Naurois[3], J.-P. Lenain[4] for the H.E.S.S. Collaboration[5]

[1]ECAP, Universität Erlangen-Nürnberg, Erwin-Rommel-Str. 1, 91058 Erlangen, Germany
[2]DESY, 15738 Zeuthen, Germany
[3]Ecole Polytechnique, CNRS/IN2P3, 91128 Palaiseau, France
[4]LPNHE, CNRS/IN2P3, 4 Place Jussieu, 75252, Paris Cedex 5, France
[5]https://www.mpi-hd.mpg.de/hfm/HESS/

January 16, 2023

**Abstract**

The purpose of this technical document is to assess the effect of a gain reduction on low- and high-level analysis results and to investigate the option of using a common lowered gain for both, dark and moonlight observations. Using a sequence of six Crab Nebula runs taken at alternating gain settings, it was shown that decreasing the gain factor from 80 to 60 Analog-to-digital counts per photo-electron (ADC/pe) has no significant effect on the telescope system sensitivity under dark-sky conditions. This result confirms expectations that such a change in gain has a comparatively small effect on the signal readout. In particular, the following results were obtained: 1. The trigger rates and event statistics are comparable for both gains. 2. The distributions of Hillas parameters are consistent for both gains. 3. The spectral analysis results are consistent within about 10%. The efficiency of detecting gamma rays is energy-independent and consistent for both gains, indicating no loss of performance at any energy.

*Corresponding author, contact.hess@hess-experiment.eu

# Contents

**1 Introduction** **2**
1.1 Technical motivation . . . 2
1.2 NSB rate, PMT gain and ageing . . . 2
1.3 NSB versus electronic noise . . . 3

**2 Reduced-gain study of back-to-back Crab Nebula observations** **3**
2.1 Strategy . . . 3
2.2 Comparison of trigger rates . . . 4
2.2.1 Pixel trigger thresholds . . . 4
2.2.2 Array trigger rates . . . 5
2.2.3 Single-telescope trigger rates . . . 6
2.3 Event statistics . . . 6
2.4 Spectral analysis . . . 10
2.5 Cross-check based on Run-Wise Simulations . . . 12

**3 Conclusion** **13**

**A Analysis configuration and detailed results** **14**

**List of Abbreviations** **14**

**Bibliography** **14**

# 1 Introduction

## 1.1 Technical motivation

Observations taken during moonlight are characterized by higher Night Sky Background (NSB) rates than those typical for observations taken during astronomical darkness. Higher NSB rates at a given Photomultiplier tube (PMT) gain lead to higher anode currents as well as higher trigger rates. The former can be controlled by lowering the PMT gain, the latter by increasing the pixel trigger threshold. In general, increased anode currents have two major effects: 1. In the short term, they may cause a pixel to be turned off if the maximum sustainable current has been reached (similarly to pixels being turned off due to the presence of bright stars in their Field of View (FoV)); 2. In the long term, they contribute to PMT ageing. Both issues can be addressed by operating the instrument at a lower PMT gain, ideally at one common lower gain factor for observations during both moonlight and astronomical darkness.
This study assesses whether and in what manner the reduction of the PMT gain affects the overall performance of the High Energy Stereoscopic System (H.E.S.S.) instrument for dark-time observations, including low- as well as high-level aspects. Only the HESS-IU telescopes, i.e. CT1-4 after the camera upgrade of 2016 [3], were included in the study, since the large CT5 telescope has been equipped with the next-generation FlashCam camera featuring different trigger strategy.

## 1.2 NSB rate, PMT gain and ageing

The gain setting for dark observations expressed in units of Analog-to-digital counts per photo-electron (ADC/pe) has been $80\,\mathrm{ADC/pe}$ up to the time of this study, performed in the first half of the year 2020. The

H.E.S.S. Moonlight Observations Group proposed then to use a common gain setting of $60\,\mathrm{ADC/pe}$ for all observations, i.e. under dark as well as moonlight NSB levels. Moonlight observations constitute 10 to 20% of the total observation time, depending on the instrument configuration and the allowed maximum moon phase and separation angle between the moon and the target source. As of January 2022, observations taken while the moon is above the horizon contribute about 17% to the overall current. By extending the lower gain factor to dark-time observations as well, the HESS-IU PMTs would operated at an optimal setting, ensuring their functioning for the remaining lifetime of H.E.S.S.

Furthermore, operation and maintenance of the instrument would be simplified significantly by keeping one common gain setting. This affects many systems, including Data acquisition (DAQ), calibration (both the number of sets of calibration runs that need to be taken and off-line calibration), Instrument Response Function (IRF) production, as well as event reconstruction. A common $60\,\mathrm{ADC/pe}$ gain factor would allow calibration to be performed in the same manner as for the original $80\,\mathrm{ADC/pe}$ gain setting. The number of needed IRF sets and data sets characterized by different systematic effects would be kept to a minimum. Further reduction of the gain factor to $50\,\mathrm{ADC/pe}$ has been investigated but found to become challenging in the description of the single photo-electron peak for about 5% of all pixels. Therefore, a 20% buffer of 10 ADC/pe is preferred to ensure that calibration procedures are not affected.

### 1.3 NSB versus electronic noise

The typical NSB flux from non-galactic-plane regions during dark time (without moonlight) induces a photo-electron rate of about $100\,\mathrm{MHz}$ per pixel in the CT1-4 telescopes [10]. This corresponds to a contribution of $1.6\,\mathrm{pe}$ in a readout window of $16\,\mathrm{ns}$. In comparison, electronic noise typically contributes about 0.2 pe per readout window.
Reducing the gain factor by 25% from $80\,\mathrm{ADC/pe}$ to $60\,\mathrm{ADC/pe}$ has the following effects on noise:

- It does not change the number of photo-electrons produced at the photo-cathode, be it induced by a Cherenkov-shower or NSB photons.
- It does decrease the number of electrons collected at the anode by a factor of 25%. Correct calibration, i.e. conversion from ADC counts to pe takes this into account.
- A 25% decrease in the total number of electrons collected at the anode leads to a relative increase in statistical fluctuations of 15%. This is assuming that electron multiplication in the dynode system is purely Poissonian in nature.
- The absolute level of the electronic noise remains unaffected, since it is largely gain-independent.
- However, the relative contribution of the electronic noise to the final signal increases slightly. For a signal equal to the pixel trigger threshold of $5.5\,\mathrm{pe}$, the relative contribution of electronic noise increases from 3.6% to 5.5%, i.e. by less than 2%.

In principle, in terms of noise and fluctuations, reducing the gain factor is equivalent to observing brighter regions of the sky. To put this in perspective: The NSB rates of dark extra-galactic fields are about $100\,\mathrm{MHz}$, in brighter galactic-disk fields approximately $200\,\mathrm{MHz}$. The increase in noise associated with doubling the NSB rate is larger than that caused by a 25% gain reduction.

## 2 Reduced-gain study of back-to-back Crab Nebula observations

### 2.1 Strategy

Aiming at changing the gain setting without a significant effect on the telescope system sensitivity under dark-sky conditions, this study assessed the effect on the signal readout. In particular, the need for scaling

the the pixel trigger threshold when adjusting the gain makes it necessary to check that the trigger rates and event statistics are comparable. In order to judge whether the efficiency of detecting gamma rays is energy-independent and consistent for both gains, the distributions of Hillas parameters, as well as the all-particle (i.e. including charged cosmic rays) and the gamma spectra are studied. The spectral analysis completes the consistency check of the results.

In order to isolate the effect of the gain setting, a total of six Crab Nebula runs were taken in succession on 18/19 January 2020 during dark time. This string of runs alternated between the run type Observation-Run (OR) ($80\,\mathrm{ADC/pe}$) and MoonlightObservationRun (MOR) ($60\,\mathrm{ADC/pe}$), with the pixel trigger threshold being $5.5\,\mathrm{pe}$ for both gain settings. The flat-fielding coefficient[1] [1] obtained from dedicated observations in the observation period P2019-11 was used to correct for different optical and quantum efficiencies of the pixels within each camera, which was done for both gain settings. Pairs of runs taken directly back-to-back are most suitable for comparative analysis like this one, as zenith angles and atmospheric conditions should be comparable. Here, the zenith angles of observations varied between 45.3 and 50.5 degrees. The atmospheric effects in particular can easily change by around 10% from one night to the next, thus back-to-back runs with no time gaps in between are crucial to minimise these effects. An overview of the observations is provided in table 1.

| Run Start Time | Gain (ADC/pe) | Zenith angle (deg) | Offset, R.A. (deg.) | Offset, Dec. (deg.) | NSB rate (MHz) | Atmosphere transparency coefficient |
|---|---|---|---|---|---|---|
| 19:19:02 | 80 | 48.2 | 0 | 0.7 | 105.64 | 1.00 |
| 19:50:04 | 60 | 45.3 | 0 | −0.7 | 117.12 | 1.26 |
| 20:18:48 | 80 | 45.4 | 0.755 | 0 | 108.10 | 1.00 |
| 20:47:41 | 60 | 46.0 | −0.755 | 0 | 114.94 | 1.27 |
| 21:16:28 | 80 | 46.7 | 0 | −0.7 | 103.40 | 1.02 |
| 21:45:19 | 60 | 50.5 | 0 | 0.7 | 117.17 | 1.30 |

**Table 1:** Table summarising the instrument and atmospheric conditions under which the six back-to-back observations of the Crab Nebula were taken. The NSB rate (calculated from the width of the pedestal distribution) and the atmospheric transparency coefficient [7] resulting from the data calibration, one of the two analysis chains used in H.E.S.S., are the mean values over the four telescopes. The transparency coefficient is systematically higher for the runs taken at the lower gain, since the muon efficiencies [5] are about 25 to 28% higher in the MORs than in the ORs, and the transparency coefficient is directly proportional to it.The muon efficiencies are higher for the runs taken at lower gain, because they are derived from the average amplitude of muon rings where the gain is assumed to still have the standard value. A comparison of an image prediction to reality results in a shifted value.

## 2.2 Comparison of trigger rates

### 2.2.1 Pixel trigger thresholds

The Crab Nebula is considered the standard candle of gamma-ray sources. Thus the measurements of its flux have historically been used to assess analysis performance and systematic uncertainties [2]. In this study, the pixel trigger threshold was adjusted in parallel with the gain, when the gain was decreased

[1] In order to correct for different responses of pixels to uniform illumination after calibration of the electronic chain, the mean signal over each camera is calculated and the ratio of each pixel signal to this mean accumulated in a histogram. The pixel efficiency relative to the camera mean is the mean of this ratio, and its inverse is called the flat-field coefficient.

by 25% from $80$ to $60\,\mathrm{ADC/pe}$. Note that the trigger threshold is generally quoted in units of pe; since one photo-electron (produced at the photo-cathode) remains one photo-electron regardless of the gain setting, the pixel trigger threshold in pe was always $5.5$. The photo-electron-value is internally converted to a voltage, which is then fed into a comparator, where the trigger decision is made. The 25% scaling was applied in this step, assuming a linear relationship between gain and threshold (this is a good first-order approximation).

Pixel threshold scans have been performed between November 2019 and January 2020 using the standard ($80\,\mathrm{ADC/pe}$) and the reduced gain factor ($60\,\mathrm{ADC/pe}$). The fact that the transition points at both gains were comparable within $0.1\,\mathrm{pe}$ indicates that the threshold scaling works well.

### 2.2.2 Array trigger rates

The array trigger rates (i.e. rates of events coincident on at least two telescopes) for both gain settings are consistent within 10%. This is illustrated in Fig. 1. For the reduced gain, a 10% increase in trigger rates is observed at comparable zenith angles, indicating that the effective pixel trigger threshold (i.e. after converting and scaling $5.5\,\mathrm{pe}$ to a voltage value) is slightly lower at the reduced gain, and thus slightly more low-energy events close to the trigger thresholds of the telescopes are recorded. Note that among this 10% higher trigger rate, a non-significant fraction of events originates in NSB triggers that later will be removed in the cleaning procedure and/or higher-level reconstruction and image or event classification. This effect is visible in the all-particle and gamma distribution plots in the analysis section further down, see Section 2.3.

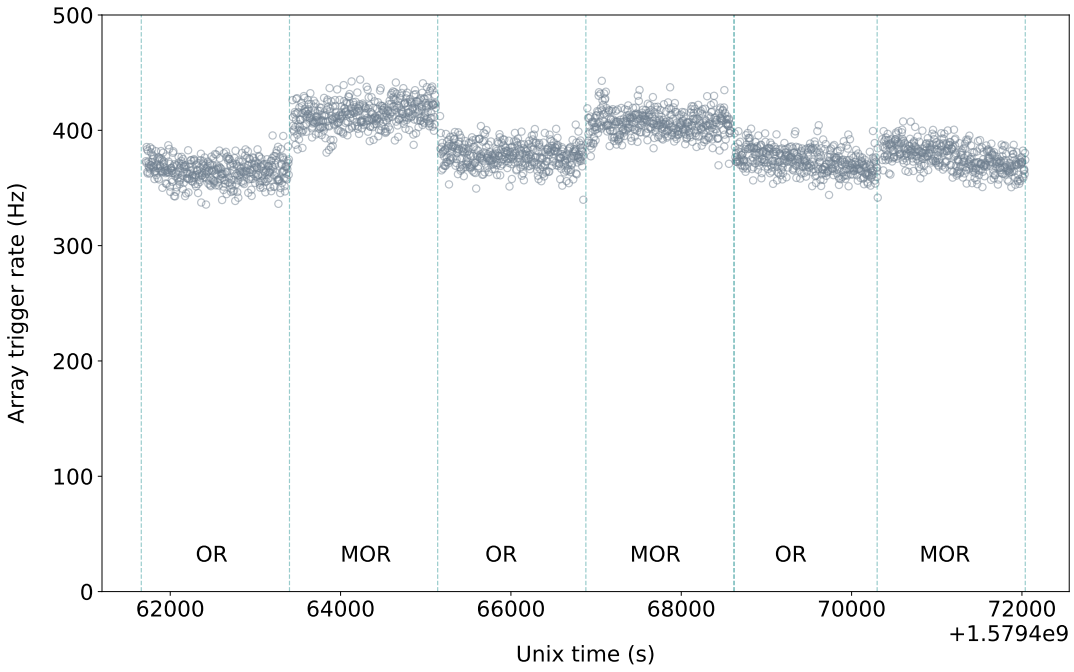


**Figure 1:** Comparison of array trigger rates for both gain settings.

### 2.2.3 Single-telescope trigger rates

The single-telescope rates at the reduced gain are elevated with respect to the standard gain by about 20%, as illustrated in Fig. 2. This is caused by two different effects:

- The slightly lower effective pixel threshold at lower gain, which was already seen in the array trigger rates.
- More pixels with bright stars in their FoV: A bright star will cause a pixel to be turned off once a critical anode current was reached. At a reduced gain setting at the moment of observations, this anode current limit was reached later, i.e. bright stars that would cause a pixel to turn off at the standard gain may not do so at the reduced gain setting, thus elevating the single-telescope trigger rates. This behavior has been improved later by adapting the limits of the pixel rate limiter algorithm.

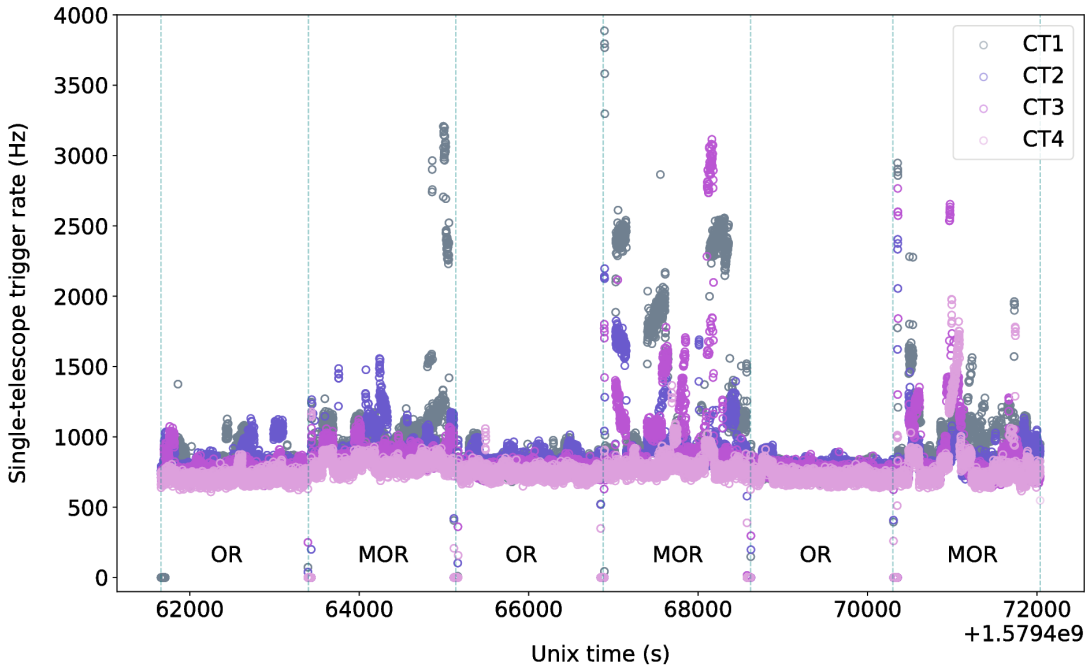


**Figure 2:** Comparison of single telescope trigger rates for both gain settings. Spikes are related to the moving of bright stars on the field of view, which can "fire" pixels for the short period of time (this is mitigated by masking pixels in the trigger).

## 2.3 Event statistics

The data taken during the six runs at two different gains were combined to obtain two data sets, one for each gain setting. The analysis results presented below were obtained by applying the ring-background method [4]. However, the reflected-background method yields consistent results with those obtained by applying the ring-background method, and was used to extract spectral results. Any effects related to the

slightly elevated level of noise and fluctuations are expected to show close to the trigger threshold, i.e. for low-size images. Since the look-up tables, gamma-hadron separation and IRFs have been optimised for a gain setting of $80\,\mathrm{ADC/pe}$, any difference between the assumed and real camera and hardware behaviour would propagate into differences in image and cut parameter distributions, as well as gamma-ray event statistics and reconstructed spectra. Note that these differences can be accounted for with an adaptation of the IRFs. Therefore, in order to isolate these potential differences, the data set was restricted to energies greater that $1\,\mathrm{TeV}$. Above this energy, a better agreement between the two gains is observed. The reduced-gain data set yields about 7% more gamma-ray events at a slightly higher significance level and with a comparable background. The event statistics for the data sets with and without the energy cut are summarised in table 2.

The distributions of Hillas parameters of cleaned images after pre-selection (with cuts on image size and distance between the image center of gravity and the camera center) are shown in Fig. 3. As expected, the distributions do not indicate the presence any significant difference in the shape of shower images.

If no separation cuts are applied to distinguish gamma-ray initiated air showers from hadronic ones, i.e. all particles are considered, then the energy distributions are consistent between the gains. At the lowest energies, where Cherenkov images have the lowest intensities, more events are reconstructed at the reduced gain, which can be explained by the slight decreasing of the threshold. The situation is the same for gamma-ray candidates (after selection cuts [9]). Fig. 4 illustrates the distributions of events as a function of energy.

| Gain and energies | Mean zenith (deg) | $N_{\mathrm{on}}$ | $N_{\mathrm{off}}$ | Excess | Significance |
|---|---|---|---|---|---|
| $80\,\mathrm{ADC/pe}$, above threshold | 46.76 | 670 | 967 | 581.52 | 35.72 |
| $60\,\mathrm{ADC/pe}$, above threshold | 47.18 | 791 | 984 | 700.61 | 40.61 |
| $80\,\mathrm{ADC/pe}$, above $1\,\mathrm{TeV}$ | 46.76 | 274 | 215 | 248.53 | 24.65 |
| $60\,\mathrm{ADC/pe}$, above $1\,\mathrm{TeV}$ | 47.18 | 292 | 206 | 268.16 | 26.33 |

**Table 2:** Summary of the event statistics of the combined data sets. $N_{\mathrm{on}}$ and $N_{\mathrm{off}}$ are so-called on- and off-counts, obtained from pointing at the source and pointing on a region of the same size not containing the source, respectively. Units for $N_{\mathrm{on}}$, $N_{\mathrm{off}}$, and excess are counts.

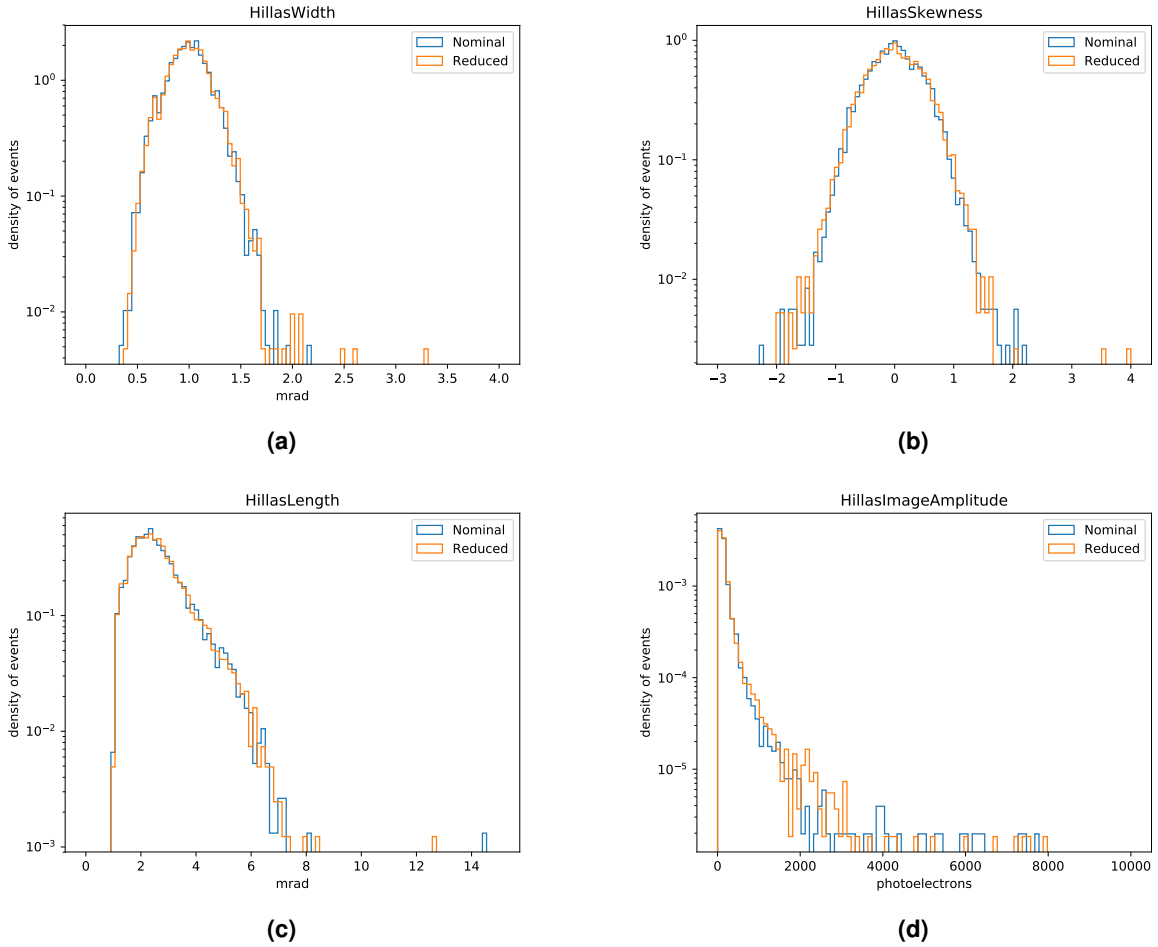


**Figure 3:** Hillas parameter distributions including a) the width, b) the skewness, c) the length, and d) the image amplitude of the ellipse after applying image cleaning and pre-selection cuts for the two data sets taken at different gains. No apparent difference in shape of shower images is seen.

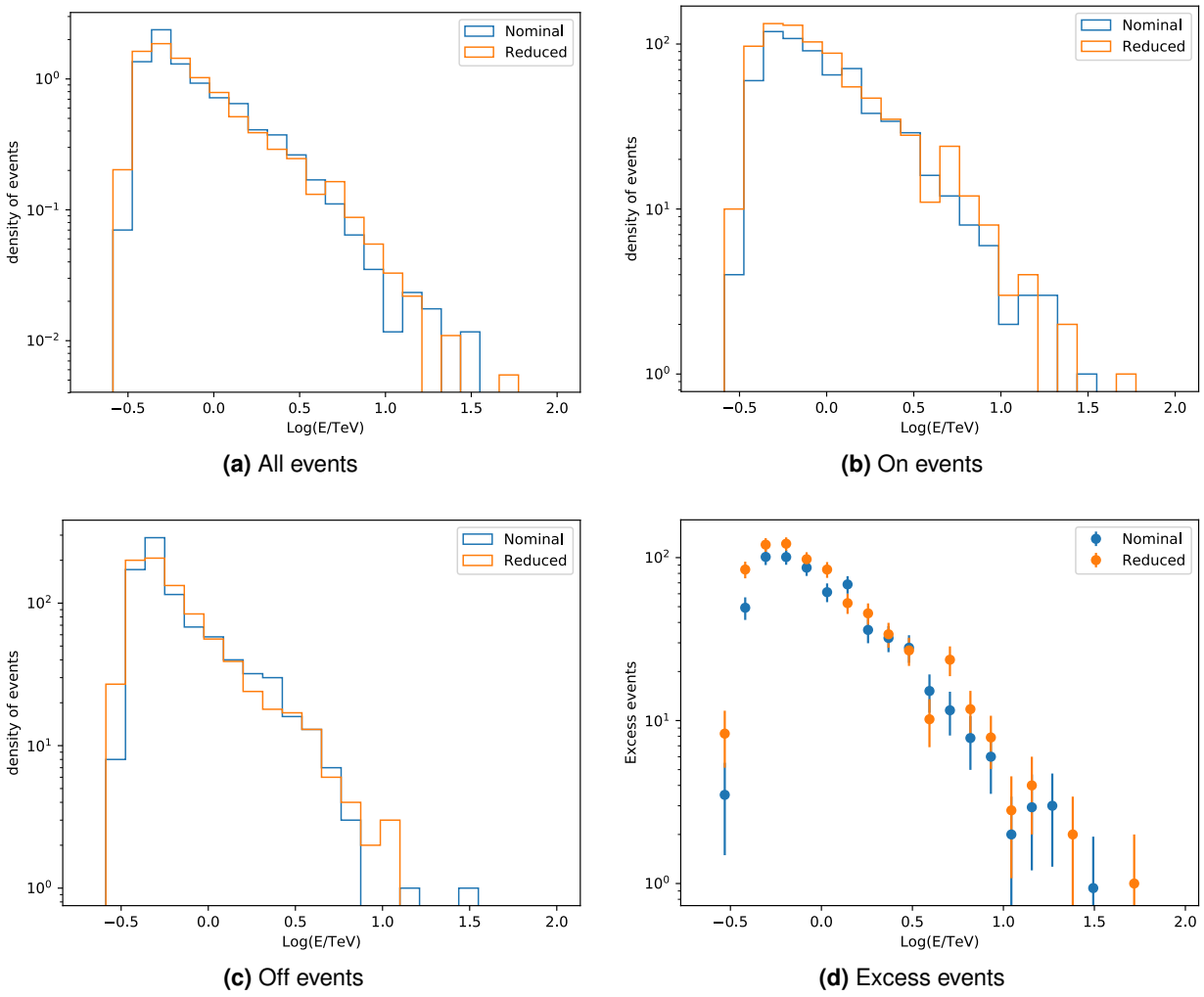


**(a)** All events

**(b)** On events

**(c)** Off events

**(d)** Excess events

**Figure 4:** Energy distributions for gamma-ray candidates at standard and reduced gain.

The fact that the event statistics (on- and off-events, as well as the excess) are consistent between the gains across the entire energy range suggests that observations of gamma-ray sources with different characteristics (e.g. weaker sources, different source spectra) will behave in a similar way.

The slight mismatch at low energies is most probably a result of a combination of effects. These include increased array trigger rates at reduced gain, using standard-gain IRFs for the reconstruction of reduced-gain data, and non-optimised Boosted Decision Tree (BDT) classification cuts. In particular the latter were optimized for standard-gain data and are expected to shift slightly for the reduced gain. The energy threshold in our analysis is based on the distribution of gamma-ray-like events as a function of reconstructed energy. Thus we obtain a slight increase of energy threshold, which may result from the first two effects. On the other side the comparison of gamma-hadron classifier outputs seen in Fig. 5 are in good agreement with each others. Overall, the agreement in spectral parameters is very good.

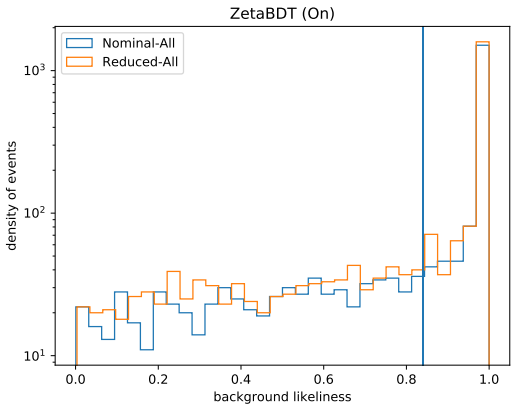


**(a)** On events

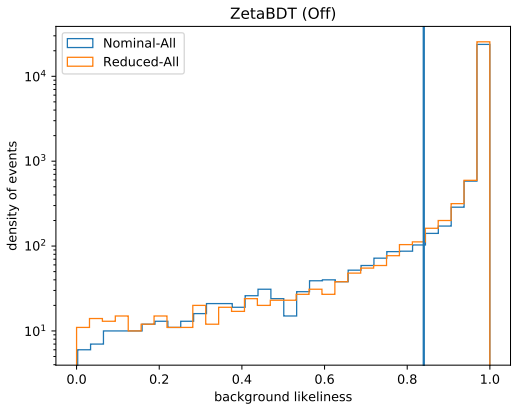


**(b)** Off events

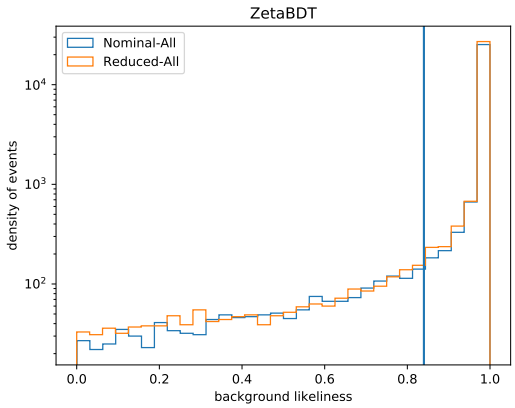


**(c)** All events

**Figure 5:** Zeta BDT distributions for gamma-ray candidates at standard and reduced gain. No gamma/hadron separation is applied to show the full distribution. The vertical line in each plot indicates the value 0.84, above which an event is classified as a hadron, whereas all events below this cut are accepted as gamma-like events.

## 2.4 Spectral analysis

Spectra have been reconstructed for all events above the analysis threshold and all events above $1\,\mathrm{TeV}$. The plot of the energy spectrum over the full energy range is shown in Figure 6.

Limiting the data set to energies above $1\,\mathrm{TeV}$ reduces the flux differences by a factor of two to three, in this case from 13% to 4%. The signal efficiency, which was found to be 10% higher for the reduced gain compared to the standard one, is consistent with the Crab Nebula flux being reconstructed to 10% higher values of integrated reconstructed flux. Spectra are consistent within 10% in flux for all energies (see table 3) and within 5% for energies above $1\,\mathrm{TeV}$. Spectral indices are in excellent agreement.
The observed differences are comparable to those found in a similar study comparing Crab Nebula runs taken at identical standard instrument settings (the former standard gain of $80\,\mathrm{ADC/pe}$), namely a study

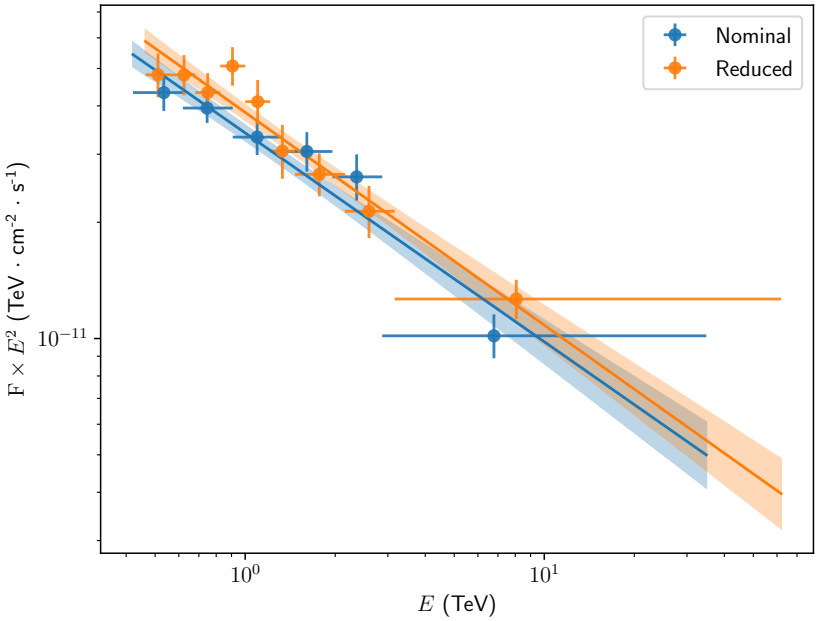


**Figure 6:** Comparison of all-energy spectra for both gain settings.

| Property | Standard gain | Reduced gain | **Red./std.** |
|---|---|---|---|
| Index | $2.54 \pm 0.06$ | $2.55 \pm 0.05$ | **1.00** |
| Thr. (TeV) | 0.42 | 0.46 | **1.10** |
| Flux above Thr. ($\mathrm{cm^{-1}\,s^{-1}}$) | $(8.35 \pm 0.406) \times 10^{-11}$ | $(8.16 \pm 0.387) \times 10^{-11}$ | **0.98** |
| Flux ($\mathrm{cm^{-1}\,s^{-1}\,TeV^{-1}}$) at 1 TeV | $(3.41 \pm 0.155) \times 10^{-11}$ | $(3.85 \pm 0.173) \times 10^{-11}$ | **1.13** |
| Flux ($\mathrm{cm^{-1}\,s^{-1}}$) above 1 TeV | $(2.20 \pm 0.118) \times 10^{-11}$ | $(2.48 \pm 0.116) \times 10^{-11}$ | **1.13** |

**Table 3:** Summary of the spectral properties of the combined data sets for all energies. The energy threshold is abbreviated as Thr., standard and reduced (gain) as std. and red.

investigating intrinsic fluctuations. The data sets were chosen such as to have comparable livetimes and zenith angles as in this reduced-gain study. Again, the runs were taken back-to-back to ensure comparable conditions as much as possible. The observed differences in the spectral parameters, i.e. energy threshold, index, and flux, are up to 20% and are comparable to the differences found in this study. This suggests that these differences originate in remaining variations in e.g. ambient observing conditions such as the atmospheric transparency, or the instrument response under nominal conditions, and how those are treated in the analysis chain and produced IRFs, rather than a difference in gain setting. The differences in the spectral parameters presented here are understood in terms of the differences in the analysis results described in this document and will be mitigated by matching Monte-Carlo simulations to the actual camera hardware settings. The source of intra-night variations are a topic of active study, are expected to be reduced significantly and will be addressed in a future technical publication.

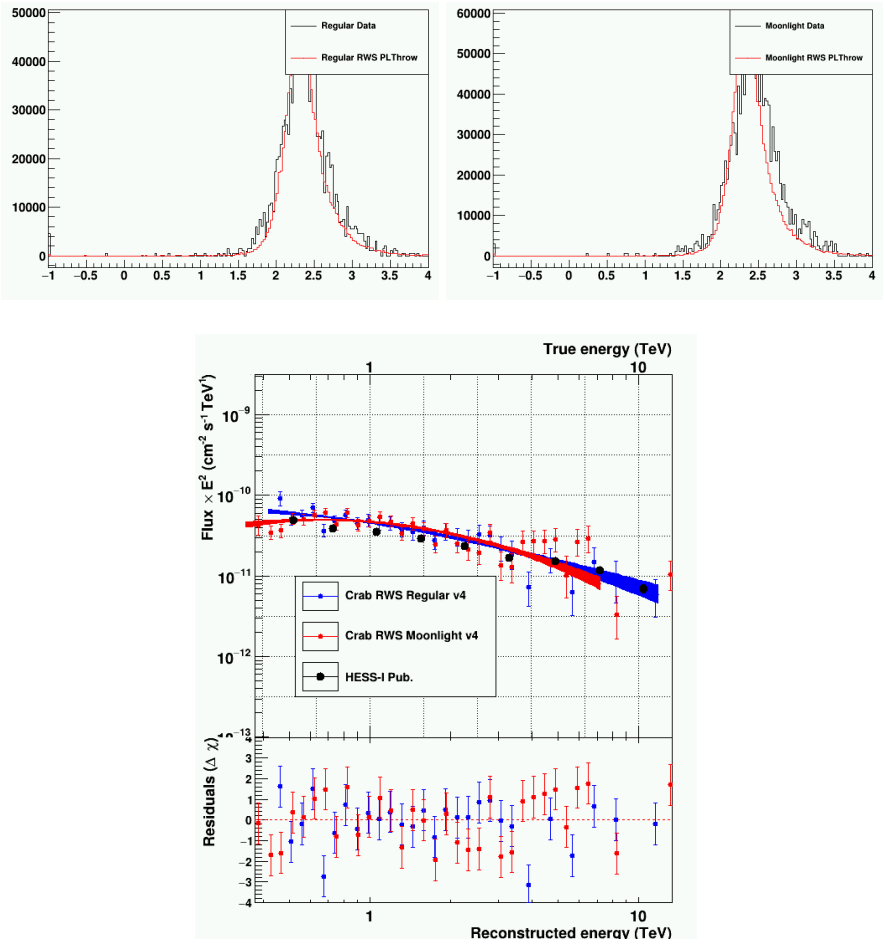


**Figure 7:** Top: Examples of charge distributions predicted by simulations (in red) in comparison to real data (in black) for the regular and reduced settings. Bottom: Spectra reconstructed using run-wise simulations.

## 2.5 Cross-check based on Run-Wise Simulations

We have performed cross-check based on independent calibration and reconstruction [6], which features so-called Run-Wise Simulations allowing for production of fine-tuned IRFs suitable for particular observations [8]. Figure 7 shows the comparison between spectra reconstructed for regular and moonlight settings, which are in agreement with each other and ones obtained by reconstruction software used in previous sections. Examples of charge distributions predicted by simulations in comparison to real data show discrepancies for moonlight data since the trigger thresholds were not adjusted for the decreased gains, as they are in the camera at the moment of this cross-check.

# 3 Conclusion

Using a sequence of six Crab Nebula runs taken at alternating gain settings, it was shown that decreasing the gain from $80$ to $60\,\mathrm{ADC/pe}$ has no significant effect on dark-time observations. This result is expected considering that such a gain reduction has minimal effects on the noise level. In particular, we have confirmed the following are consistent at both gain setting:

- The trigger rates, both single-telescope and array rates
- The event statistics (excess and significance)
- The distributions of Hillas parameters (length, width, skewness and amplitude)
- The gamma spectra (post-selection, where the likeness of an event to be of hadronic or electromagnetic origin is determined using the multivariate analysis method described in [9])
- The all-particle spectra, as well as the gamma spectra (post-selection, where the likeness of an event to be of hadronic or electromagnetic origin is determined using the multivariate analysis method described in [9])
- The spectral analysis, e.g. the flux, energy threshold and spectral indices, are consistent within 10%.
- The efficiency of detecting gamma rays is energy-independent and consistent for both gains, strongly indicating no loss of performance at any energy.

Since the look-up tables, gamma-hadron separation and IRFs have been optimised for a gain setting of $80\,\mathrm{ADC/pe}$, any difference between assumed and real camera and hardware behaviour will propagate into differences in image parameter distributions, cut parameter distributions, and finally gamma-ray event statistics and reconstructed spectra. An adaptation of the IRFs will account for these differences.

# Acknowledgements

The support of the Namibian authorities and of the University of Namibia in facilitating the construction and operation of H.E.S.S. is gratefully acknowledged, as is the support by the German Ministry for Education and Research (BMBF), the Max Planck Society, the German Research Foundation (DFG), the Helmholtz Association, the Alexander von Humboldt Foundation, the French Ministry of Higher Education, Research and Innovation, the Centre National de la Recherche Scientifique (CNRS/IN2P3 and CNRS/INSU), the Commissariat à l'Énergie atomique et aux Énergies alternatives (CEA), the U.K. Science and Technology Facilities Council (STFC), the Knut and Alice Wallenberg Foundation, the Polish Ministry of Education and Science, agreement no. 2021/WK/06, the South African Department of Science and Technology and National Research Foundation, the University of Namibia, the National Commission on Research, Science & Technology of Namibia (NCRST), the Austrian Federal Ministry of Education, Science and Research and the Austrian Science Fund (FWF), the Australian Research Council (ARC), the Japan Society for the Promotion of Science, the University of Amsterdam, and the Science Committee of Armenia grant 21AG-1C085. We appreciate the excellent work of the technical support staff in Berlin, Zeuthen, Heidelberg, Palaiseau, Paris, Saclay, Tübingen and in Namibia in the construction and operation of the equipment. This work benefited from services provided by the H.E.S.S. Virtual Organisation, supported by the national resource providers of the EGI Federation.

# A Analysis configuration and detailed results

The analysis configuration and run-wise spectral analysis results which are documented on the page linked below is internal H.E.S.S. information that can be made available upon request.
https://hess-confluence.desy.de/confluence/x/FwA5BQ

# List of Abbreviations

**ADC/pe** Analog-to-digital counts per photo-electron

**BDT** Boosted Decision Tree

**DAQ** Data acquisition

**FoV** Field of View

**H.E.S.S.** High Energy Stereoscopic System

**IRF** Instrument Response Function

**MOR** MoonlightObservationRun

**NSB** Night Sky Background

**OR** ObservationRun

**PMT** Photomultiplier tube

# Bibliography

[1] F Aharonian et al. “Calibration of cameras of the HESS detector”. In: *Astroparticle Physics* 22.2 (2004), pp. 109–125.

[2] Felix Aharonian et al. “Observations of the Crab nebula with HESS”. In: *Astronomy & Astrophysics* 457.3 (2006), pp. 899–915.

[3] Terry Ashton et al. “A NECTAr-based upgrade for the Cherenkov cameras of the HESS 12-meter telescopes”. In: *Astroparticle Physics* 118 (2020), p. 102425.

[4] David Berge, S Funk, and J Hinton. “Background modelling in very-high-energy $\gamma$-ray astronomy”. In: *Astronomy & Astrophysics* 466.3 (2007), pp. 1219–1229.

[5] Raphaël Chalmé-Calvet, M de Naurois, and J-P Tavernet. “Muon efficiency of the HESS telescope”. In: *arXiv preprint arXiv:1403.4550* (2014).

[6] M. de Naurois and L. Rolland. “A high performance likelihood reconstruction of $\gamma$-rays for imaging atmospheric Cherenkov telescopes”. In: *Astropart. Phys.* 32 (Dec. 2009), pp. 231–252. DOI: 10.1016/j.astropartphys.2009.09.001. arXiv: 0907.2610 [astro-ph.IM].

[7] J Hahn et al. “Heidelberg Data Quality Selection”. In: *HESS internal note* (2013).

[8] M. Holler et al. “A Run-Wise Simulation and Analysis Framework for Imaging Atmospheric Cherenkov Telescope Arrays”. In: *Astropart. Phys.* 123 (2020), p. 102491. DOI: 10.1016/j.astropartphys.2020.102491. arXiv: 2007.01697 [astro-ph.HE].

[9] Stefan Ohm, Christopher van Eldik, and Kathrin Egberts. "$\gamma$/hadron separation in very-high-energy $\gamma$-ray astronomy using a multivariate analysis method". In: *Astroparticle Physics* 31.5 (2009), pp. 383–391.

[10] S Preuß et al. "Study of the photon flux from the night sky at La Palma and Namibia, in the wavelength region relevant for imaging atmospheric Cherenkov telescopes". In: *Nuclear Instruments and Methods in Physics Research Section A: Accelerators, Spectrometers, Detectors and Associated Equipment* 481.1-3 (2002), pp. 229–240.